# Eliminating spiral waves pinned to an anatomical obstacle in cardiac myocytes by high-frequency stimuli

Akihiro Isomura,[1] Marcel Hörning,[1] Konstantin Agladze,[1,2] and Kenichi Yoshikawa[1,*]
[1]*Department of Physics, Graduate School of Science, Kyoto University and Spatio-Temporal Project, ICORP JST, Kyoto 606-8502, Japan*
[2]*Institute for Integrated Cell-Material Sciences (iCeMS), Kyoto University, Kyoto 606-8501, Japan*
(Received 16 July 2008; published 24 December 2008)

The unpinning of spiral waves by the application of high-frequency wave trains was studied in cultured cardiac myocytes. Successful unpinning was observed when the frequency of the paced waves exceeded a critical level. The unpinning process was analyzed by a numerical simulation with a model of cardiac tissue. The mechanism of unpinning by high-frequency stimuli is discussed in terms of local entrainment failure, through a reduction of the two-dimensional spatial characteristics into one dimension.

DOI: 10.1103/PhysRevE.78.066216 PACS number(s): 05.45.−a, 87.19.Hh, 87.18.Hf

## I. INTRODUCTION

Rotating spiral waves of activity have been observed in many biological, physical, and chemical systems [1–4]. Many of the studies on these phenomena have been inspired by the relevance of this topic to the functioning of the heart under normal and pathological conditions [5–7]. Rotating waves are believed to be responsible for many dangerous cardiac tachyarrhythmias and are precursors of ventricular fibrillation and subsequent sudden death (reviewed in Ref. [8]). Thus, the development and improvement of methods to terminate rotating waves would be an important contribution to this field of medicine. Existing techniques are typically based either on high-energy shocks or a train of low-energy high-frequency pulses [9]. The latter method is preferred because the less-intense stimulation current minimizes tissue damage and patient trauma. The present study is focused on this issue.

The application of a train of stimuli to terminate tachycardia before it proceeds to fibrillation is called antitachycardia pacing (ATP) [10]. Although it is very often a successful and justified medical procedure, the mechanism of ATP is not yet sufficiently understood and modifications to improve ATP are based on empirical rather than mechanistic considerations. Recent experiments with cultured cardiac myocytes have shown that one plausible mechanism of spiral wave termination by ATP is induced drift of the rotating wave and collision with the unexcitable border of the tissue [11]. The main claim against this mechanism of spiral wave termination may be that a pathological rotating wave is not a "free spiral" but rather a "pinned spiral" in the heart tissue. Due to the highly heterogeneous nature of the heart tissue, spiral waves tend to attach to the local heterogeneities and are stabilized as pinned rotating waves [12,13]. Tung and co-workers convincingly demonstrated the spontaneous pinning of rotating spirals to relatively small obstacles in cardiac myocytes [14]. Thus, unpinning of rotating waves from anatomical obstacles is an important prerequisite for the successful application of ATP. In the present study, we examined the dynamics of spiral waves pinned to anatomical obstacles in cultured cardiac myocytes as well as their unpinning by the high-frequency pacing.

## II. MATERIALS AND METHODS

### A. Experimental methods

Primary cell cultures of neonatal rat ventricular myocytes were prepared as described elsewhere [15]. Briefly, hearts that had been isolated from one-day old Wistar rats were minced and treated with collagenase. The isolated cells were collected by centrifugation and preplated for 1 h. After the supernatant was collected again, the cells were plated on 22-mm diameter glass coverslips coated with fibronectin (12 $\mu$g/ml) at a cell density of $2.6\times10^3$ cells/mm$^2$ with a plating medium (Dulbecco-modified Eagle medium with 10% fetal bovine serum, 1% penicillin streptomycin) and incubated for 24 h under humidified conditions at 37 °C and 5% $CO_2$. The medium was then replaced with a contraction medium (minimum essential medium with 10% calf serum, 1% penicillin streptomycin), and the cells were incubated under the same condition.

Excitation waves were observed 4–6 days after culturing. The medium was exchanged with Tyrode's solution, which includes 180 $\mu$M lidocaine, and kept at room temperature during the observations in order to decrease the wave speed. Cells were labeled with a $Ca^{2+}$ sensitive fluorescent dye, Fluo-4. Fluorescent light was observed by an inverted microscope (IX-70; Olympus) in combination with $\times1.25$ (PLAPON, numerical aperture=0.04; Olympus) low-magnification objective lenses and $\times0.35$ intermediate lens. Free spiral waves were generated by premature or rapid pacing stimuli. We applied electric rectangular pulses by using a monopolar electrode, not only for the generating free spiral waves but also for periodic pacing stimuli. The monopolar electrode was located far away from the obstacle, so as to avoid the direct interaction with the refractory region of the pinned spiral wave.

Raw images were taken by an EMCCD (iXon DV887ECS-UVB; Andor) with $128\times128$ pixels by $4\times4$ binning, 14-bit resolution, and 100 fps. Acquisition data

*yoshikaw@scphys.kyoto-u.ac.jp

 

were processed with ImageJ image-analysis software [16], using custom plug-ins. Time-series data of each pixel were temporal low-pass filtered with a cutoff frequency of 5.0 Hz for noise reduction, and Gaussian spatial convolution was applied with a 1.0 pixel radius. Finally, upstrokes of cell activation were detected and an activation time map [17] was calculated.

### B. Numerical methods

We used the Fenton-Karma model [18] for numerical simulations by replacing the step functions by the sigmoid functions [19]. The Fenton-Karma model consists of three variables: membrane potential ($u$), fast gate variable ($v$), and slow gate variable ($w$).

$$\frac{\partial u}{\partial t} = \nabla \cdot (D \nabla u) - J_{FI}(u;v) - J_{SO}(u) - J_{SI}(u;w), \quad (1)$$

$$\frac{\partial v}{\partial t} = \frac{\mathcal{S}(u_c - u)}{\tau_v^-(u)}(1 - v) - \frac{\mathcal{S}(u - u_c)}{\tau_v^+} v, \quad (2)$$

$$\frac{\partial w}{\partial t} = \frac{\mathcal{S}(u_c - u)}{\tau_w^-}(1 - w) - \frac{\mathcal{S}(u - u_c)}{\tau_w^+} w, \quad (3)$$

where the three currents $J_{FI}$ (fast inward current), $J_{SO}$ (slow outward current), and $J_{SI}$ (slow inward current) are given by

$$J_{FI}(u;v) = -\frac{\mathcal{S}(u - u_c)}{\tau_d} v(1 - u)(u - u_c), \quad (4)$$

$$J_{SO}(u) = \frac{\mathcal{S}(u_c - u)}{\tau_o} u + \frac{\mathcal{S}(u - u_c)}{\tau_r}, \quad (5)$$

$$J_{SI}(u;w) = -\frac{w}{2\tau_{SI}}\{1 + \tanh[k(u - u_c^{SI})]\}, \quad (6)$$

$$\tau_v^-(u) = \mathcal{S}(u - u_v)\tau_{v1}^- + \mathcal{S}(u_v - u)\tau_{v2}^-, \quad (7)$$

and $\mathcal{S}(u) = [1 + \tanh(k_u u)]/2$, where $k_u = 50$.

The parameters are $\tau_r = 50.0$, $\tau_{SI} = 44.84$, $\tau_o = 8.3$, $\tau_v^+ = 3.33$, $\tau_{v1}^- = 1000.0$, $\tau_{v2}^- = 19.2$, $\tau_w^+ = 667.0$, $\tau_w^- = 11.0$, $u_c = 0.13$, $u_v = 0.055$, $g_{FI} = 2.47$, and $u_c^{SI} = 0.85$. For the other parameters, $\Delta t = 0.02$ (ms), the grid size $\Delta x = 0.01$ (cm), the diffusion coefficient $D = 0.001$ (cm$^2$/ms), and the system size is $5.12 \times 5.12$ (cm). We chose a Neumann (no-flux) boundary condition for the obstacles and the boundary of the system. As the main purpose of the simulation is to make clear the scenario of unpinning, we did not make the fine tuning of the parameters so as to shift the frequency to be similar to that in the present experiment. It should be mentioned that these parameters are not tuned to the dynamics of rat cardiac tissue but capture the essential features of cardiac dynamics.

## III. EXPERIMENTAL RESULTS

Figure 1(a) shows a schematic view of the time series of fluorescent intensity obtained for a CCD pixel. We calculated

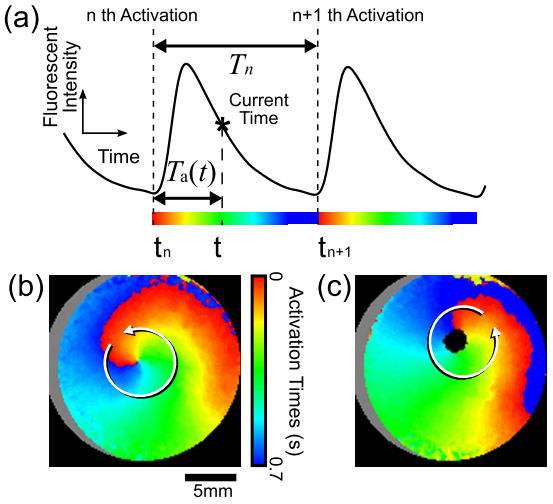


FIG. 1. (Color online) Activation time maps of rotating spiral waves in experiments of cultured cardiac myocytes. (a) Schematic view defining the local activation time $T_a(t)$ and local activation interval $T^n$. By mapping $T_a(t)$ for every pixel, we obtained activation time maps of free (b) and pinned (c) spiral waves. The curved arrows indicate the direction of rotation of the spiral wave. The black circle in (c) indicates an anatomical obstacle, where no cells exist.

the activation times and activation intervals, which are defined as shown in Fig. 1(a). The red-colored portion shows the position of the wave fronts, and propagating wave fronts were clearly visualized by the activation time maps. Figure 1(b) shows an example of a free rotating spiral wave in the activation time map. We can find a phase singularity, where almost all of the colors denoting activation times merge at the center of the spiral in Fig. 1(b). Figure 1(c) shows a pinned spiral wave attached to a millimeter-sized artificial anatomical obstacle, where the cells in the core of the free rotating spiral wave were removed surgically. There is no phase singularity in Fig. 1(c), in marked contrast to the existence of a phase singularity at the end of a free spiral wave.

With the stably rotating pinned spiral obtained, periodic pacing stimuli were applied with a frequency higher than the rotation frequency of the pinned spiral wave. Figure 2(a) illustrates an experiment in which pacing was applied from a monopolar electrode located at the position marked by an asterisk, where the natural frequency of the pinned spiral wave was 1.2 Hz.

Figure 2(b) shows the effect of pacing stimuli at 1.3 Hz. At an early stage, the collision between pinned and paced waves occurred far from the obstacle. Over the course of several cycles, the paced waves gradually shift toward the obstacle [first panel of Fig. 2(b)] and bypass the obstacle from both sides. From one side of the obstacle, the paced wave collided with the pinned spiral wave and was annihilated (dashed line in the second panel of Fig. 2). The wave that propagated through the other side of the obstacle survived and formed a new pinned spiral wave [third panel of Fig. 2(b)]. A new pinned wave then rotated around the obstacle and faced the next pacing wave [fourth and fifth panels of Fig. 2(b)]. This process was repeated at least 10 times. This repetition indicates that the system went to a steady

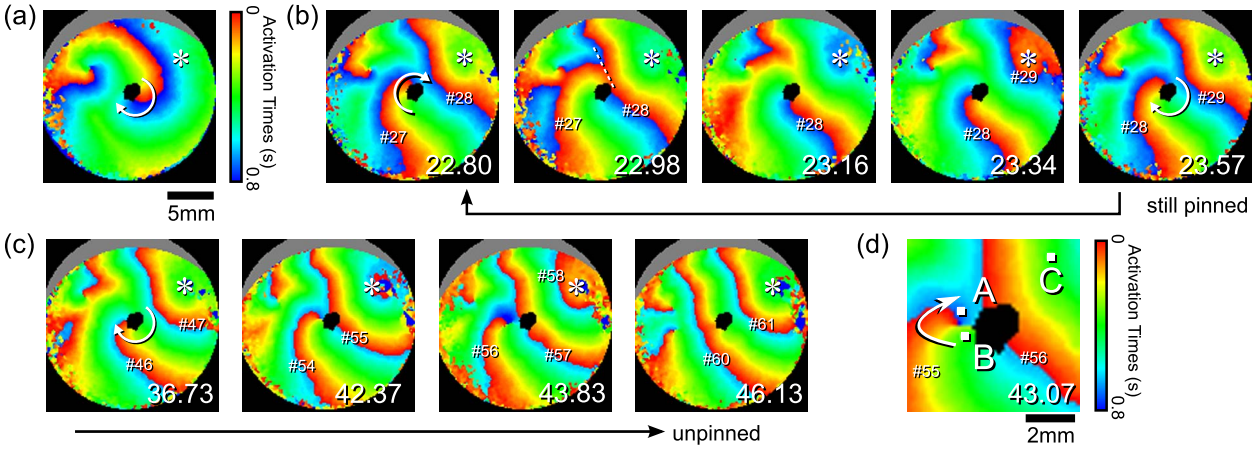


FIG. 2. (Color online) Successful and unsuccessful unpinning in experiments of cultured cardiac myocytes as a response to a high-frequency stimulus. (a) Before starting periodic pacing. The position of the pacing electrode is shown by an asterisk. The arrow indicates the rotating direction of pinned spiral wave. (b) Snapshots of unsuccessful unpinning by pacing at 1.3 Hz. (c) Snapshots of successful unpinning by pacing at 1.5 Hz. (d) Close-up view of phase singularity after successful unpinning by pacing at 1.5 Hz. Indexes such as "no. 27" indicate the wave number of the pacing wave, and other indexes such as "22.80" at the lower right of the panels indicate the time on the second time scale.

state, and thus all cells were entrained to the pacing frequency of 1.3 Hz, i.e., 0.77 s (see also Fig. 3).

Figure 2(c) shows the effect of higher-frequency pacing, when the pacing frequency was increased to 1.5 Hz for the same system. Deep blue pixels in the first panel of Fig. 2(c), which indicate longer activation intervals than the other colors, completely disappeared. Therefore, all cells were paced with lower activation intervals than before the frequency was changed. The pinned spiral wave remained anchored to the obstacle for at least five pacing cycles [first panel of Fig. 2(c)], while the position of wave annihilation gradually moved toward the obstacle. After the pacing stimulus was repeated seven times, wave No. 54 was not anchored to the obstacle and the phase singularity appeared [second panel of Fig. 2(c)], i.e., the spiral wave was detached. The detached spiral wave was paced and drifted by upcoming paced waves and finally moved away from the obstacle completely [third and fourth panels of Fig. 2(c)]. After unpinning occurred, the waves propagated around the obstacle symmetrically and no redetachment of the wave was observed [fourth panel of Fig. 2(c)]. Figure 2(d) shows a close-up image of a phase singularity. A discrete gap of activation time appeared at the region between $A$ and $B$ in Fig. 2(d). This gap means that wave No. 54 was able to pass through region $A$ but not through the region between $A$ and $B$. Therefore, the propagation of wave No. 54 was blocked in the region between $A$ and $B$ and the wave bypassed in the direction of the arrow, as shown in the right panel of Fig. 2(d). Such a gap in an activation time map reflects a conduction block, i.e., propagation failure, near the obstacle.

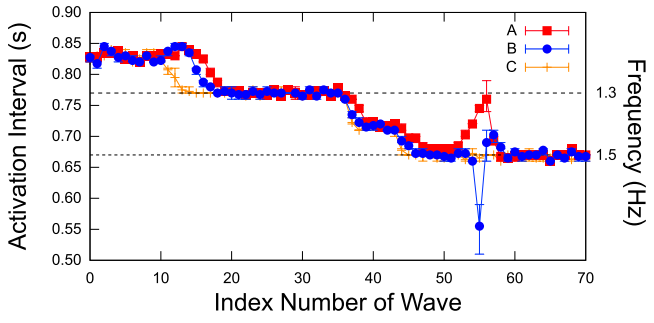


FIG. 3. (Color online) Time evolution of local activation intervals. The propagating wave was indexed and the activation intervals plotted for $A$, $B$, and $C$ shown in Fig. 2(d). Each point includes four pixels and the averaged values are shown with bars of minimum and maximum values.

To quantitatively evaluate the differences in the dynamics among the representative positions of $A$, $B$, and $C$ in Fig. 2(d), we measured the activation intervals $T_n$, which are defined as shown in Fig. 1. Figure 3 shows an entire time series of the entrainment dynamics for regions $A$, $B$, and $C$. The intervals at region $C$, which is closer to the pacing site than $A$ and $B$, were less than the others in each frame. Therefore, the cells at $C$ were synchronized to the pacing periods and there were small differences in activation intervals between $C$ and the others. On the other hand, the cells at region $B$ were synchronized to the pacing periods after entrainment at $C$. The cells at $A$ were also synchronized to the pacing periods after entrainment at $B$ in the early stage, at least before pacing wave No. 45. However, after wave No. 45, the activation intervals at region $A$ did not follow the pacing period. Finally, conduction block (i.e., propagation failure) occurred when wave No. 54 reached region $A$ and a phase singularity appeared, as shown in Fig. 2(c). At that time there is a large difference in activation intervals between region $A$ and the others. Thereafter, from wave No. 60, $A$, $B$, and $C$ were all synchronized to the pacing period. The cells at $B$ and $C$ were synchronized before the arrival of the 54th pacing wave, whereas the cells at $A$ were synchronized after the transient failure of entrainment. Therefore, there could be a correlation between the entrainment dynamics and the successful unpinning caused by a conduction block.

Application of the sufficiently high pacing frequency always led to the successful unpinning of spiral waves in our

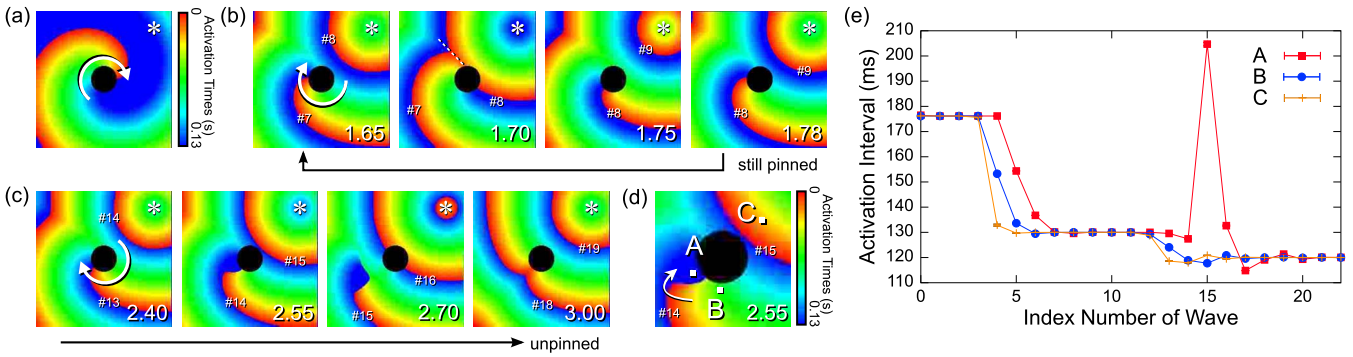


FIG. 4. (Color online) Numerical results for the unpinning process by a periodic stimulus at different frequencies. (a) Initial state before pacing. (b) Unsuccessful unpinning with periodic pacing at 130.0 ms. (c) Successful unpinning with periodic pacing at 120.0 ms. (d) Close-up snapshot. (e) Time evolution of local activation intervals.

experiments, while lower frequencies resulted in the failures on unpinning. Such an effect of the frequency was confirmed with more than ten independent experimental measurements.

## IV. NUMERICAL RESULTS

The above experimental results demonstrated the importance of wave entrainment as the basis of the mechanism of unpinning. In particular, the failure of entrainment was shown to lead to a conduction block for part of the wave front and this results in detachment of the wave from the obstacle. To obtain deeper insight into the mechanism of unpinning, we carried out numerical simulations of the unpinning of spiral waves by high-frequency pacing. Figure 4(a) shows an activation time map of a spiral wave anchored to an obstacle 6.5 mm in diameter, where the natural period of rotation is 176.1 ms. We applied electric pacing at the position marked by an asterisk in the upper-right position in the figure. Figure 4(b) shows activation time maps in the case of unsuccessful unpinning by the application of a relatively large pacing period of 130.0 ms. Figure 4(c) shows activation time maps at the moment of successful unpinning with a pacing period of 120.0 ms. These results correspond well to the experimental trends as shown in Figs. 2(b) and 2(c). The essential timing of the conduction block is given in the second panel of Fig. 4(d). The unpinned wave was then forced to drift by collisions with upcoming waves [third panel in Fig. 4(c)]. Finally, the spiral wave went away and paced waves continued to pass through the obstacle [fourth panel in Fig. 4(c)]. Figure 4(e) shows the time evolution of activation intervals at representative points *A*, *B*, and *C*. It also depicts the entrainment dynamics, which reproduce the experimental trend shown in Fig. 3.

## V. DISCUSSION

We studied the elimination of pinned spiral waves by the application of high-frequency periodic pacing by both experimental observation and a numerical simulation. For free spirals, it has been established that periodic paced waves shift the spiral core in the direction of the propagation of the paced waves. The main prerequisite for such pacing-induced drift is that the frequency of pacing must exceed the frequency of the rotating spiral wave [11,20]. This condition is obviously not sufficient for removal of the pinned spiral wave. In the case of a pinned spiral wave, successful elimination of the spiral waves must be based on two consecutive processes: unpinning of the spiral wave from the obstacle and subsequent pacing-induced drift. Therefore, successful ATP by high frequency pacing can be described as (1) approach of paced waves to the obstacle, (2) local conduction block (i.e., propagation failure) near the obstacle, (3) detachment of the wave from the obstacle, (4) pacing-induced drift, and (5) elimination at the boundary. The conduction block in the vicinity of the obstacle is the crucial step in successful unpinning. It "erases" the fragment of the wave front adjacent to the obstacle. The phenomenon of propagation failure induced by high-frequency pacing at the obstacle might be interpreted in terms of a critical (minimum) velocity, curvature-dependent wave propagation, and a dispersion relation.

It is well known that there is a critical (minimum) velocity for the successful propagation of excitation waves [21,22]. Thus, the phenomenon of propagation failure may be associated with a decrease in the velocity of the wave front near the obstacle to an unstable critical value. A detailed discussion of the estimation of the critical velocity will be presented elsewhere [23]. A decrease in wave velocity could be caused by two factors: an increase in front curvature and high-frequency pacing.

Regarding the first factor, the wave velocity depends on the wave front curvature in two-dimensional excitable media [21,24]. When a new incoming paced wave attaches to an obstacle, the velocity decreases because of the curvature effect due to deformation of the wave front. Furthermore, the curvature of the wave front increases closer to the center of a spiral wave. Since the obstacle acts as a core for the pinned spiral wave, it is expected that the velocity of wave fronts near the obstacle is always smaller and reaches the critical minimal velocity sooner than that of wave fronts in the outer region. In fact, we observed propagation failure just near the obstacle. Therefore, we can focus on the wave dynamics in the local region near the obstacle, for example, a one-dimensional circle around the obstacle.

Second, we observed that, after the pinned spiral wave was detached, the next arriving waves bypassed the obstacle

from both sides without propagation failure. This means that the wave velocity reached the critical velocity transiently during the unpinning process. Thus, it is necessary to discuss the time course of the wave velocity. For simplicity, bearing in mind the abovementioned characteristics of entrainment, we discuss the one-dimensional system near the obstacle and define the position of the pacing site as $x=0$. Thus, we will consider the one-dimensional projection on two-dimensional unpinning dynamics to grasp the essence of the mechanism of unpinning. It takes a certain amount of time for a pacing wave to reach a distant site $x$ from the pacing site. In the one-dimensional case, the $n$th activation interval at $x$, $T_n(x)$, is

$$T_n(x) = \tau + \int_0^x \left\{ \frac{1}{c_{n+1}(x')} - \frac{1}{c_n(x')} \right\} dx', \tag{8}$$

where $c_n(x)$ is the conduction velocity of the $n$th wave at position $x$ [25,26]. By differentiating, we obtain

$$\frac{dT_n(x)}{dx} = \frac{1}{c_{n+1}(x)} - \frac{1}{c_n(x)}. \tag{9}$$

This equation indicates that the spatial gradient of the activation interval reflects the change in wave velocity. If $dT_n(x)/dx$ is positive, the local velocity of the subsequent wave $[c_{n+1}(x)]$ is less than that of the previous wave at the same local position $[c_n(x)]$. Hence, there is an important relationship between the entrainment dynamics of the activation interval and wave speed. In both cases, as shown in Figs. 3 and 4, the activation intervals at position $A$ were higher than those at position $B$ before the detachment of spiral waves. After detachment, the activation intervals at positions $A$ and $B$ became equal to each other. According to Eq. (9), these results elucidate that the wave velocity decreases just before the unpinning of spiral waves. As a result, the velocity became less than critical wave velocity transiently, which leads to the propagation failure near the obstacle and subsequent detachment. In other words, it is apparent that the change in the wave velocity is the essential factor toward the achievements of successful unpinnings. The detailed mechanism of the transient decrease in the wave velocity in unpinning dynamics is still an important issue. It has been determined that the speed of wave propagation decreases as the pacing period (i.e., activation interval) decreases in excitable media (dispersion relation) [22]. In cardiac tissue, the dynamics of wave velocity are based not only on the dispersion relation but also on restitution properties [27,28]. Our observed dynamics of the wave velocity could be fully explained with the aid of a detailed theoretical consideration.

## VI. CONCLUSIONS

We studied the mechanisms of the unpinning and removal of a spiral wave as a plausible mechanism of ATP. The unpinning of spiral waves from anatomical obstacles was observed on cultured cardiac myocytes. The results showed that the pacing frequency should be larger than a critical frequency for successful unpinning. The experimental trend was reproduced by a numerical simulation. The mechanism of successful unpinning was discussed in terms of entrainment failure in a one-dimensional system, which is considered to be a reduction of the essential features of a two-dimensional spiral wave.

## ACKNOWLEDGMENTS

The authors would like to thank Dr. Valentin Krinsky (Max Planck Institute), Mr. Masanobu Tanaka (Kyoto University), and Dr. Hiroyuki Kitahata (Chiba University) for their helpful discussions.

[1] G. Gerisch, Curr. Top Dev. Biol. **3**, 157 (1968).
[2] A. T. Winfree, Science **175**, 634 (1972).
[3] M. A. Allessie, F. I. Bonke, and F. J. Schopman, Circ. Res. **33**, 54 (1973).
[4] K. Agladze and O. Steinbock, J. Phys. Chem. A **104**, 9816 (2000).
[5] V. I. Krinsky, Biophys. J. **11**, 776 (1966).
[6] G. K. Moe and J. Jalife, Arch. Inst. Cardiol. Mex. **47**, 206 (1977).
[7] A. T. Winfree, *When Time Breaks Down: The Three-Dimensional Dynamics of Chemical Waves and Cardiac Arrhythmias* (Princeton University Press, Princeton, NJ, 1987).
[8] J. Jalife, Annu. Rev. Physiol. **62**, 25 (2000).
[9] M. S. Wathen *et al.*, Circulation **110**, 2591 (2004).
[10] D. L. Hayes, P. A. Friedman, and M. Lloyd, *Cardiac Pacing and Defibrillation: A Clinical Approach* (Wiley, New York, 2000).
[11] K. Agladze, M. W. Kay, V. Krinsky, and N. Sarvazyan, Am. J. Physiol. Heart Circ. Physiol. **293**, 503 (2007).
[12] D. Pazo, L. Kramer, A. Pumir, S. Kanani, I. Efimov, and V. Krinsky, Phys. Rev. Lett. **93**, 168303 (2004).
[13] Y.-Q. Fu, H. Zhang, Z. Cao, B. Zheng, and G. Hu, Phys. Rev. E **72**, 046206 (2005).
[14] Z. Y. Lim, B. Maskara, F. Aguel, R. Emokpae, and L. Tung, Circulation **114**, 2113 (2006).
[15] T. Harada and A. Isomura, Prog. Theor. Phys. Suppl. **161**, 107 (2006).
[16] W. Rasband, URL http://rsb.info.nih.gov/ij/
[17] S. M. Hwang, K. H. Yea, and K. J. Lee, Phys. Rev. Lett. **92**, 198103 (2004).
[18] F. Fenton and A. Karma, Chaos **8**, 20 (1998).
[19] D. Allexandre and N. F. Otani, Phys. Rev. E **70**, 061903 (2004).
[20] V. I. Krinsky and K. I. Agladze, Physica D **8**, 50 (1983).
[21] V. G. Fast and A. G. Klebér, Cardiovasc. Res. **33**, 258 (1997).
[22] J. Keener and J. Sneyd, *Mathematical Physiology* (Springer, Berlin, 1998).
[23] M. Tanaka *et al.* (to be published).

[24] J. J. Tyson and J. P. Keener, Physica D **32**, 327 (1988).
[25] M. Courtemanche, L. Glass, and J. P. Keener, Phys. Rev. Lett. **70**, 2182 (1993).
[26] B. Echebarria and A. Karma, Phys. Rev. Lett. **88**, 208101 (2002).
[27] J. W. Cain, E. G. Tolkacheva, D. G. Schaeffer, and D. J. Gauthier, Phys. Rev. E **70**, 061906 (2004).
[28] E. G. Tolkacheva, J. M. B. Anumonwo, and J. Jalife, Biophys. J. **91**, 2735 (2006).